Formation and Characterization of Self-Assembled Films of Thiol-Derivatized Poly(Dimethylsiloxane) on Gold

Mei-Wei Tsao,*,† Karl-Heinz Pfeifer,‡ and John F. Rabolt†

IBM Almaden Research Center, San Jose, California 95120

David G. Castner

Box 351750, Department of Chemical Engineering, University of Washington, National ESCA and Surface Analysis Center for Biomedical Problems, Seattle, Washington 98195

Lukas Häussling and Helmut Ringsdorf

University of Mainz, Mainz, Germany

Received January 29, 1997; Revised Manuscript Received July 3, 1997[⊗]

ABSTRACT: Poly(dimethylsiloxane) (PDMS) copolymers containing propanethiol side chain "stickers" for forming self-assembled films on gold surfaces have been studied by various experimental techniques including ellipsometry, contact angle measurements, FT-IR, angle-dependent XPS, and ToF−SIMS. The results show that the thiol-containing side chains do not all chemisorb to the gold surfaces. In addition, the concentration of these sticker units was found to have a dominant effect on the polymer film thickness, the surface wetting properties, and the orientation of the PDMS backbone. Ab initio calculations reveal that the IR-active PDMS Si−O stretching bands can be used as indications of chain orientation, and a comparison of the calculated spectra with grazing incidence reflection IR data shows that the self-assembled PDMS backbone is predominantly aligned parallel to the surface, plausibly as a result of the chemisorption.

Introduction

Poly(dimethyl siloxane) (PDMS) is one of the most widely used polymers in the field of biomedical applications, and it has found more uses related to surface behavior in other areas such as the semiconductor and automobile industry.[1−4] Many of these applications are related to the unique surface properties of PDMS and its low glass transition temperature, T_g. The flexible but robust Si−O backbone together with the low intermolecular interaction of the methyl groups give PDMS a soft and stable surface with relatively low surface tension, near zero shear viscosity, and high water repellence. Unlike most other polymers such as polyolefins and fluorocarbon polymers which either degrade or form rigid glassy or crystalline structures at high and low temperatures, linear PDMS exists in a stable liquid form from above 300 °C down to about −125 °C with only minor dependence on the molecular weight. Cyclic and cross-linked PDMS can provide further modification in mechanical properties. These unique properties make PDMS extremely useful in many technical applications.

Self-assembled monolayers (SAMs)[5] films have drawn a significant amount of attention from scientists in the past decade not only because they provide a well-defined two-dimensional model system for the studies of thermodynamics and kinetics of molecules in confined geometries but also because they provide new ideas for potential applications based upon chemical and physical phenomena at the nanometer scale. The ease of formation of SAMs makes them extremely attractive for low-cost industrial coating processes while the ability to functionalize SAM species, on the other hand, provides opportunities for highly sophisticated surface applications that require precise control of the interfacial properties such as wetting, adsorption, charge transfer, and molecular alignment.[6−9]

In this study, the properties of self-assembled films formed with thiol-modified linear PDMS has been investigated. Two closely related self-assembled polymer systems have been reported by Stouffen and McCarthy (PS)[10] and Lenk et al. (PMMA).[11] Both of these systems were studied below their T_g (at room temperature), and therefore the resulting films are glassy as compared with the rubbery PDMS films used in this study. Recently Grainger et al.[12] have also reported studies on a self-assembled, low molecular weight, cyclic PDMS system. Comparison with these earlier studies will be described in the related sections of this paper.

In addition ab initio calculations have been utilized in this study to assign some of the infrared spectroscopic features of the PDMS oligomers. New features of the software package Mulliken[13] were used to identify the nature of different vibrational bands,[14] and the results show that the two IR bands at around 1100 cm^{-1}, commonly assigned as Si−O stretching modes of PDMS, actually can be used as indicators for the chain orientation. This is due to the difference in the directions in which the dipole moments change during these two types of Si−O stretching. More ab initio studies on the origin of the flexibility of PDMS chains will be discussed later in a theoretical paper.

Experimental Section

A. Sample Preparation. Poly(dimethylsiloxane) samples of different degrees of thiol derivatization were purchased from United Chemical Technologies, Inc. ($M_n \approx 7{,}800$; $M_w/M_n \approx 1.94$) and were used without further purification. Figure 1 shows the molecular structure of the three thiol-modified PDMS samples used in this study. Glass microscope slides (3 in. × 1 in.) were cleaned by acid etching followed by degreasing in isopropyl alcohol vapor and further dried under a warm nitrogen flow. Vapor deposition of 200 Å of chromium under

† Current address: Materials Science Program, University of Delaware, Newark, DE 19716.

‡ Current address: Dr. Karl Thomae GmbH, Biberach, Germany.

⊗ Abstract published in *Advance ACS Abstracts,* September 1, 1997.

S0024-9297(97)00126-5 CCC: $14.00

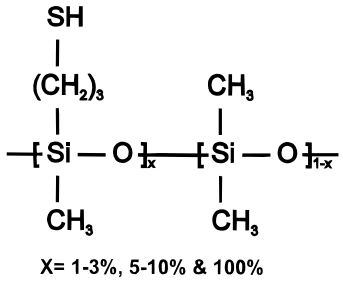

Figure 1. Molecular structure of the thiol-modified poly(dimethylsiloxanes) used for the formation of SAMs in this study.

vacuum ($\sim 5 \times 10^{-6}$ Torr) was followed by evaporation of 2000 Å of gold. The deposition rate for chromium was 4−5 Å/s and that for gold was 8−10 Å/s. Gold substrates prepared in this manner were dipped in the polymer solutions within 30 min after the substrates were removed from vacuum. Solutions were prepared with 0.1 mg/mL of PDMS in dichloromethane. Dipping time was maintained at 45 ± 1 h; at such a long dipping time, the kinetic effects on film properties due to the polydispersity of the polymer samples were tested and shown to be irrelevant. Samples were rinsed with solvent after being taken out of the solutions and then dried by a dry nitrogen flow.

B. FT-IR. All infrared measurements were made with an IBM/Bruker Model 98 evacuable FTIR at a resolution of 4 cm^{-1}. A grazing angle external reflection geometry of 83° was used to record the spectra of these thin films on gold surfaces. In order to increase the signal-to-noise ratio, 8000 scans were taken for each sample. Reference gold surfaces used in this study were covered with a self-assembled film of deuterated octadecanethiol. This coating procedure prevents the gold reference from being contaminated by airborne impurities which will interfere with the thin film IR signal.

C. Contact Angles and Ellipsometry Measurements. Static, advancing, and receding contact angles were measured with a Ramé-Hart Model 100-00 goniometer using syringe-driven water droplets. Film thickness measurements were carried out on a Rudolph Research AutoEL ellipsometer using a 6328 Å He−Ne laser output at a 70° angle of incidence. Since the refractive index of PDMS varies only slightly with its molecular weight, i.e., $n = 1.396-1.404$ over the range of $M_n = 100-20000$, we used $n = 1.40$ for the thickness evaluation of PDMS in this study.[1]

D. X-ray Photoelectron Spectroscopy. The X-ray photoelectron spectroscopy (XPS) experiments were done on a Surface Science Instruments X-probe spectrometer (SSI, Mountain View, CA). This system has a monochromatic Al Kα X-ray source ($h\nu = 1486.6$ eV), hemispherical analyzer, and resistive strip, multichannel detector. The XPS binding energies (BE) were referenced by setting the BE of the $Au4f_{7/2}$ peak to 84.0 eV. The high resolution C1s and S2p spectra were acquired at an analyzer pass energy of 50 eV. XPS elemental compositions were obtained using a pass energy of 150 eV. At this pass energy the transmission function of the spectrometer was assumed to be constant.[15] The peak areas were normalized by the number of scans, points per eV, Scofield's photoionization cross sections,[16] and sampling depth. The sampling depth was assumed to vary as $KE^{0.7}$, where KE is the kinetic energy of the photoelectrons.[15]

XPS data were acquired at nominal photoelectron takeoff angles of 0, 55, and 80°. The takeoff angle was defined as the angle between the surface normal and the axis of the analyzer lens system. For determination of a compositional depth profile (CDP), the solid acceptance angle of the analyzer lens was decreased from its normal value of 30° to 6° × 12° by placing an aperture over the analyzer lens to improve the depth resolution at each takeoff angle.[17] The regularization method of Tyler et al.[18] was used to generate a CDP from elemental compositions measured at each takeoff angle. The mean free paths used to generate the CDPs were calculated from the equations given by Seah and Dench.[19]

E. Time-of-Flight Secondary Ion Mass Spectrometry. The time-of-flight secondary ion mass spectrometry (ToF−SIMS) data were acquired using a Model 7200 Physical Electronics instrument (PHI, Eden Prairie, MN). The 8 keV Cs^+ ion source was operated at a current of 1.5 pA and a pulse width of 0.9 ns. Data were acquired over a mass range from $m/z = 0$ to 1000 for both positive and negative secondary ions. The ion beam was moved to a new spot on the sample for each spectrum. The total ion dose used to acquire each spectrum was less than 2×10^{12} ions/cm^2. The area of analysis for each spectrum was 0.01 mm^2. The secondary ions were extracted into a two-stage reflectron time-of-flight mass analyzer with a potential of 3 kV. A secondary ion focusing lens between the analyzer entrance and drift region was held at 1 kV, promoting high angular acceptance and good transmission of ions. The band pass of the analyzer is 100 eV, and an independent adjustable grid voltage (deceleration) allows energy focusing to be performed. The ions were post-accelerated to 10 kV and converted to charge pulses by a stacked pair of chevron-type multichannel plates (MCP). The signals were detected using a 256 stop time-to-digital converter (TDC) with 156 ps time resolution. The typical mass resolution ($m/\Delta m$) for both positive and negative secondary ions was 5000.

The mass scale for the negative secondary ions was calibrated using the CH (13.0078), C_2H (25.0078), SiO_2 (59.9668), and Au (196.9665) peaks. The mass scale for the positive secondary ions was calibrated using the $SiCH_3$ (43.0040), SiC_3H_9 (73.0474), $Si_2OC_5H_{15}$ (147.0661), $Si_3O_3C_5H_{15}$ (207.0329), and $Si_4O_4C_7H_{21}$ (281.0517) peaks. The fit between the expected and observed masses for both positive and negative calibration ions was less than 20 ppm.

Table 1. Properties of Thiol-Derivatized PDMS Absorbed Films

	thickness (Å)	θ_s (deg)	θ_{adv} (deg)	θ_{rec} (deg)
1−3% SH−PDMS	42 ± 3	102 ± 4	103 ± 2	101 ± 3
5−10% SH−PDMS	32 ± 3	101 ± 4	103 ± 2	97 ± 3
100% SH−PDMS	19 ± 2	82 ± 4	95 ± 3	78 ± 4
bulk PDMS (spun)		101 ± 3	103 ± 2	92 ± 3

Results and Discussion

A. Ellipsometry and Contact Angle Measurements. Table 1 shows the macroscopic properties of the self-assembled PDMS films with different percentages of thiol-derivatized side groups, together with that of a spun PDMS bulk film. The data show that the film thickness decreases as the concentration of the thiol "sticker" groups increases. The 100% SH PDMS, with one propyl thiol group on every monomeric unit, is more tightly bound to the gold surface than the other two samples. However, the static water contact angle data indicate that the 100% SH PDMS film has the highest hydrophilicity, a property which most likely results from the thiol groups exposed to the surface since thiol-terminated surfaces give water contact angle on the order of 80°.[20] The self-assembled 1−3% and 5−10% SH PDMS films, on the other hand, show water contact angles which are very close to that of a bulk, non-cross-linked PDMS surface (92−103°). Dynamic water contact angle measurements show that the 1−3%, 5−10%, and 100% SH PDMS films exhibit a hysteresis of 2, 6, and 17°, respectively. Here the increasing hysteresis is attributed to an increase of compositional heterogeneity on the different surfaces due to the increase of thiol group concentration.[21] It is worthwhile to point out that the contact angle hysteresis of 2° for the linear 1−3% SH PDMS film is as low as that of a surface of tightly cross-linked PDMS films, which constitute one of the most important families of surfaces in applications that require high water-repellence.[1] One of the reasons for this unusual property of thiol-derivatized PDMS films may be due to the orientation of the PDMS chains when they are self-assembled to the surface. The anchored and therefore more oriented film structure reduces the

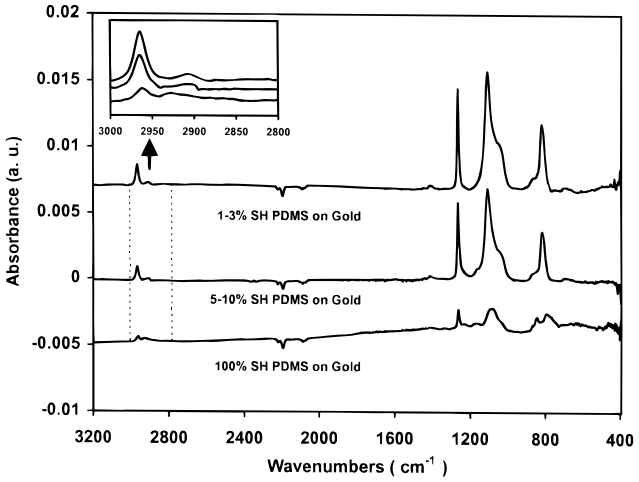

Figure 2. Grazing incidence reflection IR spectra of PDMS SAMs taken at 83° angle. Each spectrum is composed of 8000 scans.

extent of reorganization of the film when put in contact with the advancing or receding water droplets during the contact angle measurements. In contrast, a free standing polymer film with low degree of cross-linking has a higher tendency to undergo structural reorganization when put in contact with water, and this reorganization could change the dynamic aspects of the wetting angles significantly. There are other factors such as the film thickness, which could also have caused the low water contact angle hysteresis observed on the SAM formed from 1−3% SH PDMS. However, since both the underivatized PDMS film cast on gold and the 1−3% SH PDMS film cast on zinc selenide with similar thickness as the self-assembled 1−3% SH PDMS (4 nm), i.e., physisorbed PDMS films formed without self-assembly, show large contact angle hysteresis (>10°) just like the spun PDMS bulk film shown at the bottom of Table 1, the immobilization of the PDMS chain due to self-assembly is considered the main reason for the observed low hysteresis of 1−3% SH PDMS film on gold surface.

B. Polarized Infrared Spectroscopy. Grazing incidence reflection IR measurements were made on PDMS samples with three different thiol concentrations and the spectra of the self-assembled PDMS films are shown in Figure 2. In the CH stretching region (inset, Figure 2), the 1−3% SH spectrum shows only the symmetric and asymmetric CH_3 stretching bands at 2907 (ν_s) and 2965 (ν_a) cm^{-1}, respectively. There is no sign of the CH_2 stretching bands' presence due to the low concentration of the CH_2-containing propyl groups in this sample. The 5−10% SH spectrum shows similar CH stretching behavior in this region. The 100% SH sample, on the other hand, shows both CH_3 and CH_2 stretching bands in this region. The CH_3 bands shows up at 2904 (ν_s) and 2962 (ν_a) cm^{-1}; the CH_2 bands show up at 2854 (ν_s) and 2926 (ν_a) cm^{-1}. These latter bands appear at 2850 and 2920 cm^{-1} on conformationally ordered long chain hydrocarbons, and hence from these data one can conclude that no close packing of the hydrocarbons can occur under these conditions.[22]

In the region of 2000−2300 cm^{-1}, absorption bands in the negative direction (down) are present in all three spectra shown in Figure 2. These bands are due to the deuterated octadecanethiol molecules self-assembled onto the reference gold surfaces. These SAM layers prevent the physisorption of airborne hydrocarbons which interfere with the spectroscopic measurements, and the use of a deuterated SAM also prevents any intensity contributions in the CH stretching region.

In the region below 2000 cm^{-1}, all bands can be divided into three major groups. In the 1200−2000 cm^{-1} region, both the 1−3% SH and the 5−10% SH films show the asymmetric bending of the CH_3 group (δ_a) at 1414 cm^{-1} and the symmetric bending of the CH_3 group (δ_s) at 1265 cm^{-1}. Both of these bands show up in the 100% SH spectrum with significantly weaker intensities at 1413 (δ_a) and 1264 (δ_s) cm^{-1}, respectively. In the 900−1200 cm^{-1} region, all three samples show strong bands around 1100 cm^{-1} which have been attributed to the Si−O stretching.[23,24] Two bands are observed in the 1−3% SH at 1110 and 1050 cm^{-1}, with the latter being a shoulder. The 5−10% SH exhibits two bands at 1109 and 1045 cm^{-1} (shoulder), while the 100% SH sample, due to its high degree of side chain sticker concentration and its consequent deviation from regular PDMS, shows a doublet at 1094 and 1083 cm^{-1}, plus a weak shoulder at the low frequency end. Although this spectral behavior of the 100% SH PDMS differs from that of the 1−3% SH and 5−10% SH PDMS in this region, the bands here are still believed to be related to the Si−O stretching, only with different substituents on the Si−O backbones. Finally, in the region below 900 cm^{-1}, the CH_2 and CH_3 rocking bands are predominant. In 1−3% SH, the CH_2 rocking shows up as a shoulder at 865 cm^{-1} with the CH_3 rocking band at 820 cm^{-1} having the greatest intensity. Similar behavior is observed in the 5−10% SH spectrum with the CH_2 rocking vibration at 865 cm^{-1} (shoulder) and the CH_3 rock at 819 cm^{-1}. In the 100% SH, the intensities of the CH_2 rocking at 848 cm^{-1} and CH_3 rocking at 796 cm^{-1} are comparable due to the increased CH_2 group concentration from the sticker groups. This change of composition contributes greatly to the intensity of the CH_2 rocking band which appears only as weak shoulders in the other two samples.

In addition to the general spectroscopic features mentioned above, there are several important features in Figure 2 worth pointing out. First, the overall spectral intensities of the three different samples reflect their thickness difference accurately in that the thicker 1−3% SH PDMS has the largest volume sampled by the IR beam and therefore shows the highest IR spectral intensities while the thinner films show lower spectral intensities. When the contribution from the difference in film orientation is excluded, the sampling conditions are nearly identical for all measurements. This can be best shown by the identical C−D stretching band intensities (~2200 cm^{-1}) due to the deuterated octadecanethiol-coated reference surfaces. Second, the different degree of chemical modification of each sample can be monitored by the change in IR band positions; e.g., the change of the Si−O frequency reflects the heavily altered chemical linkage in the 100% SH PDMS. Third, the relative intensities of each band change with both the orientation of the polymers and the relative concentration of the species that give rise to the band. Although it is quite straightforward to see the concentration effects, the effects of orientation on the relative intensities are more subtle and therefore require a more detailed understanding of the nature of each band. To this end, we focused our attention on the Si−O stretching vibrations which are present in the IR spectra of all Si−O containing species, including PDMS. A series of ab initio calculations were undertaken utilizing Mulliken software. The IR frequency−intensity result was obtained following a geometrical optimization process at either the Hartree−Fock or MP2 level of theory using either a 3-21G* or DZP basis set. A detailed

Table 2. Ab Initio Calculation Results of Different Siloxane-Containing Systems

Si−O containing species modeled	level of theory/basis set	asym str, cm^{-1} (exptl 1050 cm^{-1})	sym str, cm^{-1} (exptl 1110 cm^{-1})
$H_3Si-O-SiH_2-O-SiH_3$	RHF/3-21G*	1141	1151
$H_3Si-O-SiH_2-O-SiH_3$	RHF/DZP	1102	1117
$H_3Si-O-SiH_2-O-SiH_3$	MP2/DZP	1143	1145
$H_3Si-O-(SiH_2-O)_3-SiH_3$	RHF/3-21G*	1131	1157
$H_3Si-O-(SiH_2-O)_3-SiH_3$	RHF/DZP	1089	1122
$Si(CH_3)_3-O-Si(CH_3)_2-O-Si(CH_3)_3$	RHF/3-21G*	1090	1118
$Si(CH_3)_3-O-Si(CH_3)_2-O-Si(CH_3)_3$	RHF/DZP	1034	1070

description of this calculation can be found in a later paper.[25] The system calculated was $(CH_3)_3Si-O-Si(CH_3)_2-O-Si(CH_3)_3$, a 37-atom molecular analog of PDMS. Hydrogenated species such as $H_3Si-O-SiH_2-O-SiH_3$ were also studied to compare with the dimethyl species, and due to the reduction in the number of atoms and consequently the lower CPU requirement, longer hydrogenated siloxanes were calculated to study the chain length dependence of the calculated vibrational bands. In all the molecules calculated, there indeed exist two strong bands in the 1100 cm^{-1} region.[26] Upon further analysis, these two bands have been shown to be due to the symmetric (higher frequency) and asymmetric (lower frequency) stretching modes of Si−O bonds. The dynamic viewing method used for the identification of each mode has been described previously.[14] The results from the dimethylsiloxane species fall within 50 cm^{-1} when using different basis sets (3-21G* and DZP). The same type of basis set dependence was observed on the hydrogenated species, with the more complicated DZP basis set giving frequency results closer to the experimental values. In the chain length dependence test with the hydrogenated species, the frequency difference between the shorter " Si−O−Si−O−Si" species and the longer "Si−O−Si−O−Si−O−Si−O−Si" species is less than 20 cm^{-1}. This indicates that the vibration characteristics of Si−O bonds depends little on the length of the chain sequence. On the other hand, the frequency difference of Si−O stretching modes between the dimethylsiloxanes and the hydrogenated species is less than 100 cm^{-1}, indicating that both Si−O stretching modes are localized vibrations and thus quite independent of the substituents attached to the silicon atoms. Finally, the difference between SCF and MP2 levels of theory is also within 100 cm^{-1}, again indicating the robustness of these two calculated stretching bands. Most important of all, the high frequency mode is found to be consistently associated with the symmetric stretching vibration of the Si−O bond, while the lower frequency component is always associated with the asymmetric Si−O stretching. Table 2 shows the calculated Si−O stretching frequencies for different systems and Figure 3 shows the comparison between the calculated IR spectrum and an experimental IR spectrum for bulk PDMS.[27] Figure 4 shows the orientation of the change in dipole moment associated with the two Si−O stretching modes. In Figure 4 it is shown that the net dipole moment change is parallel to the chain direction for the asymmetric mode and perpendicular to the backbone for the symmetric Si−O stretch. The results from this calculation can now be used to analyze the chain orientation in the self-assembled PDMS films.

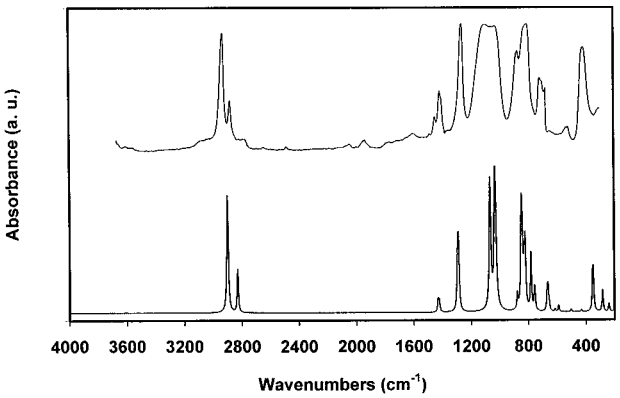

Figure 3. Comparison between the calculated (lower trace) and experimental (upper trace) IR data for PDMS. The calculation is done on $(H_3C)_3-Si-O-Si(CH_3)_2-O-Si-(CH_3)_3$ using a SCF level of theory with the DZP basis set. The experimental data is adapted from ref 27.

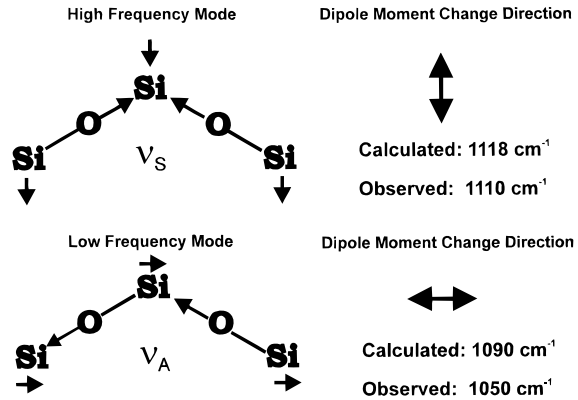

Figure 4. Illustration of the change of dipole moment directions in the two calculated Si−O vibrational modes.

C. Orientation in Self-Assembled PDMS Films. To decide the chain orientation of PDMS SAM, two grazing incidence reflection IR spectra of 1−3% SH PDMS are compared. In Figure 5, the dotted spectrum is taken with PDMS cast film on gold, while the solid spectrum was obtained from PDMS self-assembled on gold. Both films have similar thickness (on the order of a few nanometers) so that the sampling depth issue associated with the grazing incidence reflection will not interfere with the observation. Figure 5 clearly shows that the ratios of the two Si−O stretching bands are different in the two cases; the high frequency mode is significantly enhanced in the self-assembled films. The same type of behavior of PDMS on surfaces has also been observed by other workers.[28] From the results of the ab initio calculation previously discussed, this observation supports the notion that the dipole moment change associated with the symmetric stretching vibration is aligned approximately normal to the gold surface; i.e., the PDMS chains are predominantly parallel to the surface when self-assembled onto the gold surface. The cast film, on the other hand, remains more isotropic as in the bulk film case. Interestingly enough, the symmetric band is slightly enhanced over the asymmetric band even in the cast film case. This suggests that some thiol−gold bonding still occurs during the casting process, contributing slightly to the orientation of the PDMS chains.[29] The 5−10% SH PDMS self-assembled on gold also shows the same type of enhancement of the high frequency mode, indicating that there exists a similar orientation effect due to the self-assembly process, as in the 1−3% SH PDMS case. In the 100% SH PDMS spectrum, however, due to a combination of

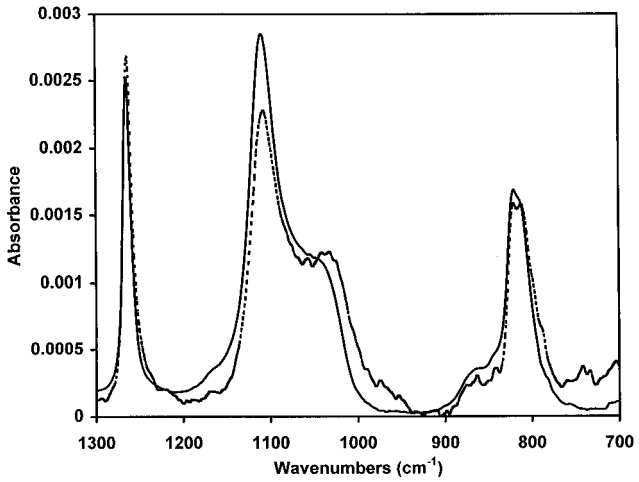

Figure 5. 700−1300 cm^{-1} grazing incidence reflection IR of PDMS on gold. The solid trace is taken from self-assembled PDMS with 1−3% SH sticker groups; the dotted trace is taken from the cast film of the same material.

Table 3. XPS Analysis of PDMS Monolayers on Gold[a]

	atomic %			
	Si	C	O	S
0% SH PDMS (theory)	25.0	50.0	25.0	0.0
1−3% SH PDMS	24.4	50.2	25.4	
5−10% SH PDMS	18.8	55.0	25.2	1.0
100% SH PDMS	11.8	63.0	18.8	6.4
100% SH PDMS (theory)	14.3	57.1	14.3	14.3

[a] The gold and sodium signals have been subtracted and the results were renormalized to provide the composition of the organic overlayer. These results were obtained at a photoelectron takeoff angle of 80°.

Table 4. Angle-Dependent XPS Gold Concentrations

	Au atomic %		
sample	80°	55°	0°
1−3% SH PDMS	5.6	15.4	26.7
5−10% SH PDMS	11.1	26.2	39.6
100% SH PDMS	14.5	30.7	44.7

heavy anchoring to the gold surface and the drastic difference in chemical structure, the Si−O stretching region could not be easily compared with that of a PDMS sample with low or no thiol modification. But for the majority of silicone-based materials with only minor modification, the above analysis provides an easy way to access the Si−O backbone orientation.

D. XPS Characterization. XPS detected the presence of Si, C, O, S, Au, and Na on all three PDMS films. The Si, C, O, S, and Au signals can be attributed to the adsorbed SH PDMS and the Au substrate. The Na signal is an unexpected contaminant, since it is not part of either the PDMS films or the Au substrate. The Na XPS concentration was between 1.5 and 3 atomic % for the three PDMS films. Table 3 shows the atomic percentages of different elements in various films. In the angle-dependent studies, the Na concentration for all PDMS/Au samples did not exhibit any significant angular dependence and therefore is not considered further in the XPS analysis. The Au signal exhibited the strongest angular dependence, and the relative strength depended on the particular PDMS film adsorbed to it (see Table 4). As the degree of thiol derivatization increases, the detected Au concentration at each takeoff angle increases. This is consistent with a decrease in the thickness of the PDMS overlayer as the percentage of thiol sticker groups increases, as

Table 5. Angle-Dependent XPS Sulfur Concentrations

	S atomic %		
sample	80°	55°	0°
1−3% SH PDMS		0.9	1.3
5−10% SH PDMS	1.0	1.9	2.2
100% SH PDMS	6.4	7.1	7.5

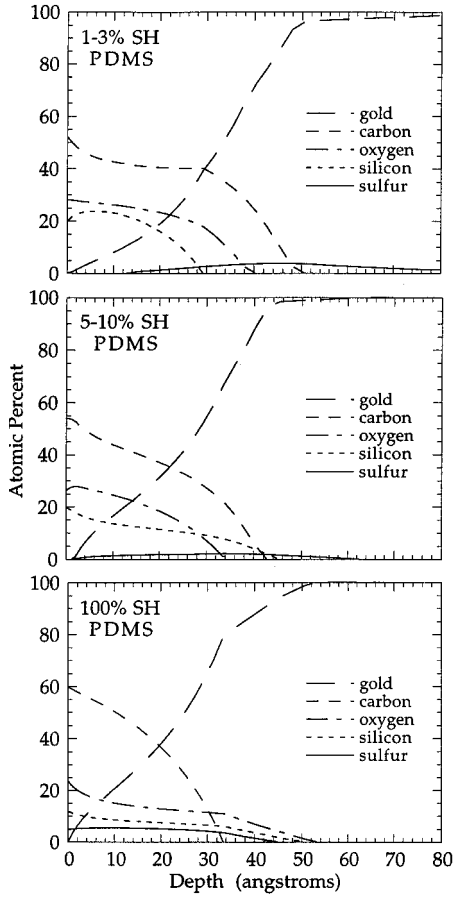

Figure 6. Composition depth profiles (CDP) generated from the angle-dependent XPS measurements of the three thiol-containing PDMS films. The thickness of the PDMS overlayer (the depth where the gold concentration reaches 50 atomic %) decreases as the thiol sticker concentration increases.

observed by ellipsometry. To examine the angular dependence of the XPS signals from the PDMS overlayer, the XPS compositions of the Au and Na signals were not included and the sum of the Si, C, O, and S concentrations were renormalized to 100 atomic %. The Si, C, and O concentrations exhibited little, if any, angular dependence. The S concentrations, especially the 1−3% and 5−10% SH PDMS films, exhibited significant angular dependence (see Table 5).

The CDPs generated from the angle-dependent XPS data are shown in Figure 6. The total thickness of the organic overlayer is given by the depth where the gold concentration reaches 50 atomic %. This depth decreased from 34 to 29 to 25 Å as the thiol sticker concentration increased from 1−3% to 5−10% to 100%. In addition to this change in overlayer thickness, the sulfur distribution also varied with the thiol sticker concentration. At the lowest thiol sticker concentration (1−3% SH), sulfur peaked at the Au interface, and no sulfur could be detected in the outer 10 Å of the film. As the thiol sticker concentration increased to 5−10% SH, the sulfur distribution extended closer to the surface film, but still no sulfur could be detected in the outermost 2 or 3 angstroms. At the highest thiol sticker concentration (100% SH), a significant sulfur concentra-

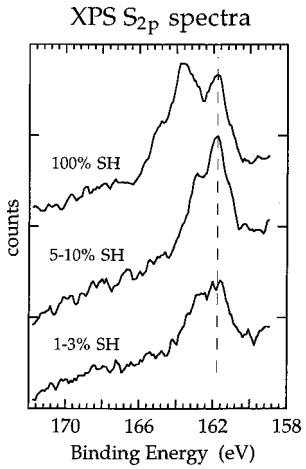

Figure 7. XPS S2p spectra from the three SH PDMS films obtained at a photoelectron takeoff angle of 0°. Peaks due to bound thiol ($S2p_{3/2}$ BE = 161.9 eV, $S2p_{1/2}$ BE = 163.1 eV) and unbound thiol ($S2p_{3/2}$ BE = 163.8 eV, $S2p_{1/2}$ BE = 165.0 eV) are observed.

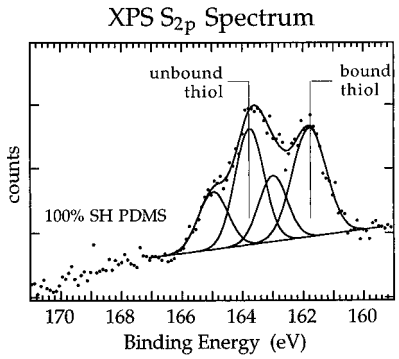

Figure 8. XPS S2p spectrum from the 100% SH PDMS film obtained at a photoelectron takeoff angle of 0° showing the peak fitting results for bound and unbound thiol species.

tion was detected at the film surface. These results are consistent with the significant decrease in the water contact angle observed for the 100 SH% PDMS film. This is the only film where the XPS CDPs indicate thiol groups are present at the outermost surface.

The high resolution S2p spectra from the three PDMS films (Figure 7) are also consistent with most, if not all, of the thiol sticker groups in the 1−3% SH and 5−10% SH PDMS films bound to the Au substrate. Sulfur $2p_{3/2}$ and $2p_{1/2}$ peaks with BEs of 161.9 and 163.1 eV, consistent with the formation of a gold−thiolate bond,[30] were observed in the spectra from these two films and accounted for at least 90% of the total spectral intensity. In contrast, a significant amount of unbound thiol ($S2p_{3/2}$ BE of 163.8 eV) was detected in the spectrum from the 100% SH PDMS film. From the peak fitting results (Figure 8) obtained by setting the $2p_{3/2}$ to $2p_{1/2}$ area ratio to 2.0 and the $2p_{3/2}$ − $2p_{1/2}$ BE splitting to 1.2, the ratio of bound to free thiol was determined to be approximately 1:1 for the 100% SH PDMS film. In the XPS studies of the sulfide-derivatized PMMA (S−PMMA) SAMs on gold surfaces reported by Lenk et al.,[11] the composition of both samples, namely 1% and 10% S−PMMA, showed no depth dependence; i.e., the sulfide "sticker" units were dispersed throughout the film thickness. This is dramatically different from the results of PDMS SAMs with similar sticker concentrations (1−3% SH and 5−10% SH) reported here. The different polymer backbones as well as the sticker groups used in these two systems are most likely the cause of this observation. On the other hand, when

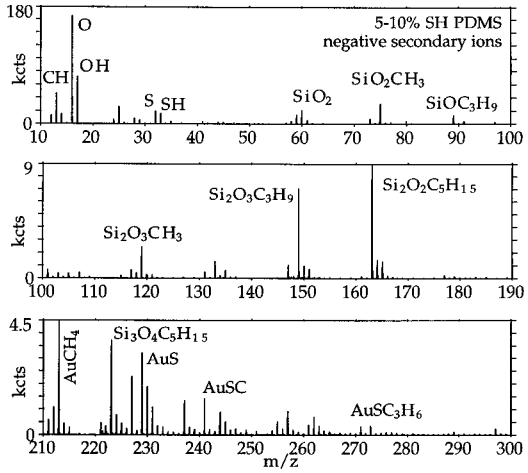

Figure 9. Low mass (m/z < 300) negative secondary ion spectrum from the 5−10% SH PDMS/Au sample. Fragments from PDMS are the primary secondary ions detected in this spectral region.

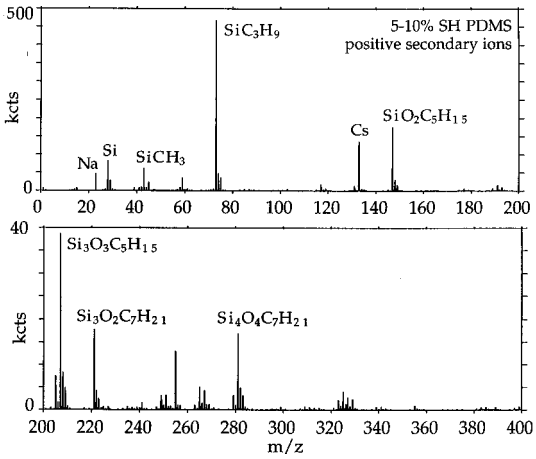

Figure 10. Positive secondary ion spectrum from the 5−10% SH PDMS/Au sample. Fragments from PDMS are the primary secondary ions detected in this spectral region.

compared with the low molecular weight cyclic PDMS with 100% thiol derivatization reported by Grainger et al.,[12] the 100% SH PDMS shows a higher percentage of bound thiol groups (ca. 50% vs ca. 33%). This is reasonable because the smaller cyclic PDMS is under significantly higher steric constraint than the linear long chain PDMS used in this study, reducing the probability for thiol stickers to reach the gold surface.

E. ToF−SIMS Characterization. The fragments below m/z = 200 in the negative secondary ion spectra were primarily from the PDMS backbone (SiO_2^- at m/z = 59.9668, $SiO_2CH_3^-$ at m/z = 74.9902, $SiOC_3H_9^-$ at m/z = 89.0420, etc.), as shown in Figure 9. In addition, S^- and SH^- ions from the thiol groups were observed along with oxidized sulfur ions (e.g., SO_3^- at m/z = 79.9568). The fact that oxidized sulfur species were detected by ToF−SIMS and not by XPS is due to the higher sensitivity of ToF−SIMS. Between m/z = 200 and 300, fragments were detected from the PDMS backbone (e.g., $Si_3O_4C_5H_{15}^-$ at m/z = 223.0278), recombination ions (e.g., $AuCH_4^-$ at m/z = 212.9977), and Au plus the thiol sticker (e.g., $AuSC_3H_6^-$ at m/z = 270.9854). Above m/z = 300, nearly all the secondary ions had the structure $Au_xS_yH_z^-$. Only the results for the 5−10% SH PDMS film are shown in Figure 9. The other two samples gave similar results, with the main difference among the samples being the variation in intensity of S^- and SH^- ions. As the concentration of thiol stickers in the film increased, so did the intensity of these

secondary ions. The entire mass range of the positive secondary ion spectra was dominated by ions from the PDMS backbone (see Figure 10). The assignments of these fragments has been discussed previously and will not be repeated here.[31,32] In addition to the PDMS fragments a peak at $m/z = 22.9898$ (Na^+) was present in the spectra from all three PDMS films.

Conclusions

This study investigates the different properties of self-assembled PDMS films. In agreement with the previous studies on sulfide-derivatized PMMA,[11] it is shown that a portion of the stickers together with the polymer chains remain dispersed throughout the film thickness of the 100% SH PDMS, with approximately a 1:1 ratio between the bound and unbound thiol groups. However, a distinct difference has been found when comparing the 1−3% SH and 5−10% SH PDMS with the sulfide-derivatized PMMA. In both PMMA samples studied (1% $S-CH_3$, 10% $S-CH_3$), the sulfur-containing sticker units were found to be dispersed evenly throughout the film thickness, while that of the PDMS with comparable degree of derivatization are predominantly bound to the gold. This differentiation between S−PMMA and SH−PDMS could be due to the different character of the binding side groups ($S-CH_3$ vs S−H) or the different mobility of the polymer backbones (glassy vs rubbery), or both. Also, as a result of the chain mobility, the self-assembled PDMS films on gold clearly exhibit a favored orientation in which the Si−O backbones lie parallel to the surfaces. The combination of ab initio calculation and polarized infrared spectroscopy proved to be a powerful technique. On the other hand, since the mobility of PDMS chains decreases with increasing anchoring of the Si−O backbone via chemisorption, therefore the 100% SH-modified PDMS forms the thinnest and least mobile self-assembled film in this study. In a separate liquid crystal alignment test,[33] both the 100% SH PDMS and PMMA SAM (crystalline film with the same thickness as 100% SH PDMS) give planar alignment to 5CB, very similar to that given by a rigid fluorinated SAM surface, while the PDMS films with lower SH percentage give homeotropic alignment, not unlike the more mobile SAM formed by mixing long/short chain alkanethiols.

The self-assembling process has been shown to have a dramatic effect on the properties of the polymer films thus formed. By control of the molecular structure of the polymeric absorbate species used in self-assembling processes, the distribution of different substituents and surface/chain interaction can be altered. The ability to modify surface structure on the nanometer scale in both the normal and lateral directions is the key to nanotechnologies. On the other hand, the multifunctional nature of polymers provides the possibilities of building a molecular integrated structure (MIS) with highly sophisticated functionalities.

Acknowledgment. M.-W.T. and J.F.R. acknowledge the support and encouragement of Dr. H. Guard of the Office of Naval Research through Contract No. N00014-93-C-0105. M.-W.T. would like to thank Prof. G. Zerbi for helpful discussion on the spectroscopy calculations. This research was also funded in part by the National Institutes of Health through grant RR-01296 (D.G.C.) for the National ESCA and Surface Analysis Center for Biomedical Problems at the University of Washington.

References and Notes

(1) Clarson, S. J.; Semlyen, J. A. *Siloxane Polymers*; PTR Prentice-Hall Inc.: New Jersey, 1993.
(2) Owen, M. J. *Ind. Eng. Chem. Prod. Res. Dev.*, **1980**, *19*, 97.
(3) Arkles, B. *CHEMTECH* **1983**, 542.
(4) Wilbur, J. L.; Kim, E.; Xia, Y.; Whitesides, G. M. *Adv. Mater.* **1995**, *7*, 649.
(5) (a) Polymeropoulos, E. E.; Sagiv, J. *J. Chem. Phys.* **1978**, *69*, 1836. (b) Sagiv, J. *J. Am Chem. Soc.* **1980**, *102*, 92. (c) Nuzzo, R. G.; Allara, D. L. *J. Am. Chem. Soc.* **1983**, *105*, 4481.
(6) Swalen, J. D.; Allara, D. L.; Andrade, J. D.; Chandross, E. A.; Garoff, S.; Israelachvilli, J.; McCarthy, T. J.; Murray, R.; Pease, R. F.; Rabolt, J. F.; Wynne, K. J. *Langmuir* **1987**, *3*, 932.
(7) Whitesides, G. M. *Chimia* **1990**, *44*, 310.
(8) Ulman, A. *An Introduction to Ultrathin Organic Films*; Academic Press: New York, 1991.
(9) Whitesides, G. M.; Ferguson, G. S.; Allara, D.; Scherson, D.; Speaker, L.; Ulman, A. *Crit. Rev. Surf. Chem.* **1993**, *3* (1), 49−65.
(10) Stouffer, J. M.; McCarthy, T. J. *Macromolecules* **1988**, *21*, 1204.
(11) Lenk, T. J.; Hallmark, V. M.; Rabolt, J. F.; Häussling, L.; Ringsdorf, H. *Macromolecules* **1993**, *26*, 1230.
(12) Sun, F.; Grainger, D. W.; Castner, D. G.; Leach-Scampavla, D. K. *Macromolecules* **1994**, *27*, 3053.
(13) Rice, J. E.; Horn, H.; Lengsfield, B. H.; McLean, A. D.; Carter, J. T.; Replogle, E. S.; Barnes, L. A.; Maluendes, S. A.; Lie, G. C.; Gutowski, M.; Rudge, W. E.; Sauer, S. P. A.; Lindh, R.; Andersson, K.; Chevalier, T. S.; Widmark, P.-O.; Bouzida, D.; Pacansky, G.; Singh, S.; Gillan, C. J.; Carnevali, P.; Swope, W. C.; Liu, B. Mulliken: a computational quantum chemistry program developed at International Business Machines Corp.
(14) Tsao, M.-W.; Pfeiffer, K.-H.; Rabolt, J. F.; Holt, D. B.; Farmer, B. L.; Interrante, L. V.; Shen, Q. *Macromolecules*. **1996**, *29*, 7130.
(15) Application notes from Surface Science Instruments, Mountain View, CA, 1987.
(16) Scofield, J. H. *J. Electron. Spectrosc. Relat. Phenom.* **1976**, *8*, 129.
(17) Tyler, B. J.; Castner, D. G.; Ratner, B. D. *J. Vac. Sci. Technol.* **1989**, *A7*, 1646.
(18) Tyler, B. J.; Castner, D. G.; Ratner, B. D. *Surf. Interface Anal.* **1989**, *14*, 443.
(19) Seah, M. P.; Dench, W. A. *Surf. Interface Anal.* **1979**, *1*, 2.
(20) Osifchin, R. G.; Mahoney, W.; Andres, R. P.; Dorogi, M.; Reifenberger, R. G.; Feng, S.; Henderson, J. I.; Bein, T.; Kubiak, C. P. *Polym. Mater. Sci. Eng.* **1995**, *73*, 208.
(21) Israelachvili, J. N. *Intermolecular & Surfaces Forces*; Academic Press: San Diego, CA 1992.
(22) Snyder, R. G.; Strauss, H. L.; Elliger, C. A. *J. Phys. Chem.* **1982**, *86*, 5145.
(23) Smith, A. L. *Spectrochim. Acta* **1963**, *19*, 849.
(24) Dobos, S.; Fogarasi, G.; Castellucci, E. *Spectrochim. Acta* **1972**, *28*, 877.
(25) Pfeiffer, K.-H.; Tsao, M.-W.; Rabolt, J. F. Manuscript in preparation.
(26) All the calculated frequencies have all been scaled by 0.89 from the raw data because SCF harmonic vibrational frequencies determined at this level of theory typically overestimate the observed fundamentals by an average of 12%. See: (a) Hehre, W. H.; Radom, L.; Schleyer, P. v. R.; Pople, J. A. *An Initio Molecular Orbital Theory*; Wiley: New York, 1986. (b) Pople, J. A.; Head-Gordon, M.; Fox, D. J.; Raghavachari, K.; Curtiss, L. A. *J. Chem. Phys.* **1989**, *90*, 5622.
(27) Data adapted from: Lin-Vien, D.; Colthup, N. B.; Fateley, W. G.; Grasselli, J. G. *The Handbook of Infrared and Raman Characteristic Frequencies of Organic Molecules*; Academic Press: San Diego, CA, 1991.
(28) Granick, S.; Soga, I. Private communication.
(29) Ren, Y.; Hoffmann, C. L.; Tsao, M.-W.; Rabolt, J. F.; Castner, D. G.; Hsu, S. L.; Häussling, L.; Ringsdorf, H. Manuscript in preparation.
(30) Castner, D. G.; Hinds, K.; Grainger, D. W. *Langmuir* **1996**, *12*, 5083.
(31) Bletsos, I. V.; Hercules, D. M.; van Leyen, D.; Benninghoven, A. *Macromolecules* **1987**, *20*, 407.
(32) Zhang, X. K.; Stuart, J. O.; Clarson, S. J.; Sabata, A.; Beaucage, G. *Macromolecules* **1994**, *27*, 5229.
(33) Miller, W. J.; Gupta, V. K.; Abbott, N. L.; Tsao, M.-W.; Rabolt, J. F. *Liq. Cryst.* **1997**, *23*, 175.

MA970126P